

FreeTacMan: Robot-free Visuo-Tactile Data Collection System for Contact-rich Manipulation

Longyan Wu^{1,4*} Checheng Yu^{1,5*} Jieji Ren^{3*} Li Chen²

Ran Huang⁴ Guoying Gu³ Hongyang Li^{2,1}

¹ Shanghai Innovation Institute ² The University of Hong Kong

³ Shanghai Jiao Tong University ⁴ Fudan University ⁵ Nanjing University

<https://opendrivelab.com/blog/FreeTacMan>

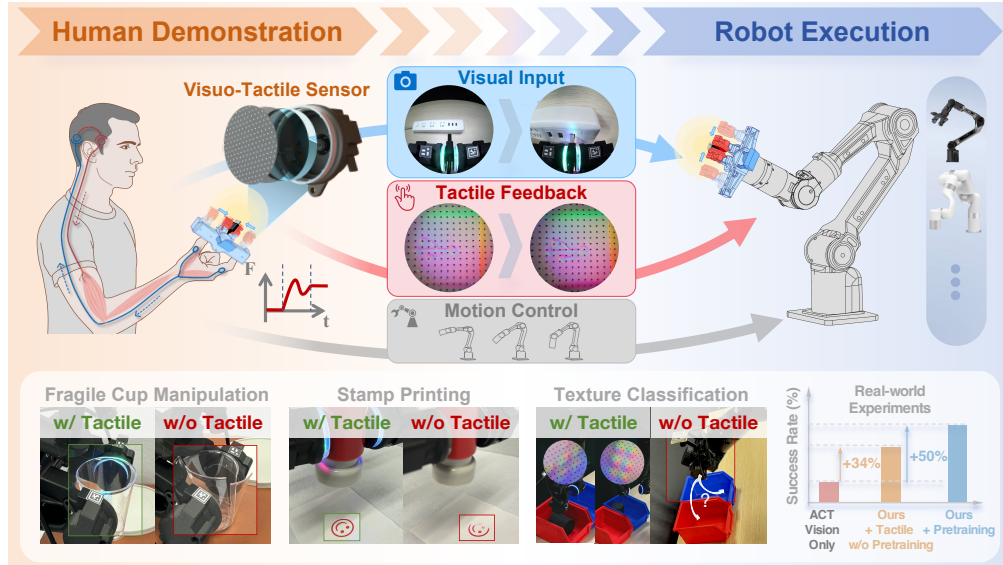


Figure 1: **Overview of FreeTacMan.** FreeTacMan is a robot-free, human-centric visuo-tactile data collection system, featuring low-cost, high-resolution tactile sensors and a portable, cross-embodiment modular design. FreeTacMan transfers human visual perception, tactile sensing, and motion control skills to robots efficiently by integrating visual and tactile data. We showcase several contact-rich manipulation tasks that are challenging for vision-only approaches.

Abstract: Enabling robots with contact-rich manipulation remains a pivotal challenge in robot learning, which is substantially hindered by the data collection gap, including its inefficiency and limited sensor setup. While prior work has explored handheld paradigms, their rod-based mechanical structures remain rigid and unintuitive, providing limited tactile feedback and posing challenges for human operators. Motivated by the dexterity and force feedback of human motion, we propose FreeTacMan, a human-centric and robot-free data collection system for accurate and efficient robot manipulation. Concretely, we design a wearable data collection device with dual visuo-tactile grippers, which can be worn by human fingers for intuitive and natural control. A high-precision optical tracking system is introduced to capture end-effector poses while synchronizing visual and tactile feedback simultaneously. FreeTacMan achieves multiple improvements in data collection performance compared to prior works, and enables effective policy learning for contact-rich manipulation tasks with the help of the visuo-tactile information. We will release the work to facilitate reproducibility and accelerate research in visuo-tactile manipulation.

* Equal contribution.

1 Introduction

Humans inherently rely on the integration of vision and touch to perform contact-rich manipulation tasks. While vision provides comprehensive object recognition and pose estimation capabilities, tactile feedback conveys critical information about local contacts that cannot be obtained visually, such as surface texture [1, 2, 3], in-hand pose [4, 5, 6], material compliance [7, 8], and force distribution [9, 10]. For example, when handling a fragile or deformable object, vision guides initial motion planning and object localization, while tactile information enables modulation of grip force and adjustment of object orientation to prevent damage.

The vision-based imitation learning has shown strong potential in robot manipulation tasks [11, 12, 13, 14], benefiting from the growing large-scale demonstration datasets [15, 16]. In the tactile domain, the lack of high-quality tactile datasets and compatible sensing hardware has prevented similar advances. Early efforts concentrated on the effectiveness of tactile information for fine-grained and contact-rich manipulation skills, with tactile data collected by sensors *attached to* robots [17, 18, 19, 20]. However, this data collection scheme limits the flexibility for scaling visuo-tactile data. To accelerate research in this domain, two prerequisites would be addressed: 1) A visuo-tactile sensor that can be fabricated and deployed at scale, and 2) a visuo-tactile data collection system that provides real-time tactile feedback and enables rapid redeployment.

As to visuo-motor sensors, existing optical tactile sensors [21, 22, 23] are often bulky, limiting their integration with diverse end-effectors, given the cost to fabricate and narrow Field of View (FoV). Moreover, they lack the modularity required for rapid adaptation across diverse embodiments. On the data collection side, some prior protocols are not optimized for high-fidelity tactile data collection. Systems that rely on motion-capture with AR/VR visualization [24, 25, 26] or primary-replica teleoperation rigs [27, 28, 29] capture accurate camera views and joint trajectories. They conversely offer no direct, real-time tactile signals, and impose fixed robot setup with complex calibration or high latency. Handheld data collection paradigms [30, 31] release the human operators from robot embodiment, and yet transmit tactile cues through long mechanical linkages, hindering direct tactile feedback and precise measurement of instantaneous tactile signals.

In this work, we introduce **FreeTacMan**, a robot-free and human-centric visuo-tactile data collection system to acquire robot manipulation data accurately and efficiently. As the basis of the visuo-tactile sensing, we develop novel internal optics and gel interface of the sensor to increase spatial resolution and FoV. To support efficient adaptation across end-effectors, the sensing module is decoupled from its mounting bracket via an electrical and mechanical connector. For the visuo-tactile data collection system that attaches the sensor, an in-situ¹ hardware structure is designed to guarantee precise, real-time tactile feedback during demonstration via two mechanisms - a gripper-finger interface coupled to human fingertips, and a linear transmission mechanism enabling precise gripper control and unattenuated tactile feedback. To validate the quality of data collected by FreeTacMan, we train and deploy imitation learning policies on challenging contact-rich manipulation tasks. Furthermore, the effectiveness of a temporal-aware tactile pretraining strategy is validated as well.

In summary, our main **contributions** are: **(i)** A portable, high-resolution, low-cost visuo-tactile hardware *sensor* designed for rapid adaptation across multiple robotic end-effectors. **(ii)** An in-situ, robot-free, real-time tactile data-collection *system* that leverages a handheld end effector and the proposed sensor to excel at diverse contact-rich tasks efficiently. **(iii)** Experimental validation shows that imitation policies trained with our visuo-tactile data achieve an average 50% higher success rate than vision-only approaches in a wide spectrum of contact-rich manipulation tasks.

¹“In-situ” indicates that FreeTacMan is designed to preserve the natural interaction between the human fingertip and the environment. It emphasizes maintaining the finger’s original grasping posture while simultaneously capturing tactile feedback. This is akin to the concept in materials science [32] and biology [33], where systems are studied in their native conditions—without altering their environment or state—to gain a deeper understanding of their behavior under actual working conditions.

Table 1: **Comparison with existing data collection systems.** The wearable, in-situ design of FreeTacMan delivers direct and high-precision tactile feedback to human operators. To evaluate tactile feedback fidelity of handheld methods quantitatively, we measure the number of mechanical transmission “link” inside the handheld gripper from human hand to the grasped object.

Category	Method	Control Method	Tactile Feedback
Teleop: VR/AR	ARCap [24]	VR Controller	–
	DexCap [25]	Hand Mocap	–
	TactAR [26]	VR Controller	Visual
	Bunny-VisionPro [34]	Hand Retargeting	Vibration
Teleop: Primary–Replica	ALPHA [28]	Puppet Arm	–
	GELLO [29]	Puppet Arm	–
	Bi-ACT [35]	Puppet Arm	Force
Handheld	UMI [30]	Trigger	Contact (4 links)
	FastUMI [31]		
In-situ	FreeTacMan (Ours)	Fingertips	Touch (1 link)

2 Related Work

Dataset Collection System for Robot Learning. Recent robot learning has been greatly advanced through imitating expert demonstrations. Popular approaches [11, 12, 36, 13] leverage large-scale visuomotor datasets (pairs of RGBD sensors and actions) to train end-to-end policies that generalize across objects and scenes. To gather data suitable for imitation learning, prior works have relied on different interfaces to teleoperate real robots, including motion capture with AR or VR visualization [24, 16, 26, 25, 34], 3D space mouse [12, 37], primary-replica system [28, 27, 29, 35], and wearable devices [38, 39, 40]. However, these setups are either expensive, operationally complex, or suffer from limited precision and require real robot control. Handheld data collection paradigms [30, 31] offer greater freedom across robot embodiment and gain access to in-the-wild data collection. Meanwhile, their trigger-based grippers and multi-link transmission designs introduce backlash between links, which blurs tactile cues and leads to inaccurate relay of gripper contact to the operator. Different from previous work, FreeTacMan implements an in-situ data collection system that enables human operators to feel gripper contact directly in real time. The comparison of control methods and approaches of tactile feedback between ours and prior work is depicted in Table 1.

Tactile Sensing for Precise Manipulation. Tactile sensing as a compensatory modality besides visual information is crucial for robot precise manipulation tasks, especially for some contact-rich manipulation tasks [41, 42, 43, 44]. Prior work on robotic tactile sensing has used force or torque sensors [45, 26, 46, 47], which are sensitive to noise and capture limited tactile information in real contact. Electrical tactile sensors can produce more realistic contact signals [48, 49, 50, 51, 52], but often suffer from low spatial resolution, crosstalk, complex fabrication, and environment interference. Camera-based visuo-tactile sensors, such as GelSight [21, 22], GelSim [23, 53], and MCTac [54], overcome these limitations by capturing the 3D deformation of a soft gel layer, achieving high resolution and capturing contact forces and surface texture. Yet, they are manufactured as one-off modules without regard for efficient adaptation onto robot end-effectors. In contrast, our visuo-tactile sensor is designed with modular interfaces both at the data collection end and the robot end-effectors, enabling rapid reconfiguration while delivering high-resolution visuo-tactile information.

3 Visuo-Tactile Data Collection System

3.1 Hardware Design

Design Criteria. To address the limitations of existing data collection systems in capturing tactile information and maintaining high-fidelity tactile feedback, as well as the issues of bulky size and limited FoV in current visuo-tactile sensors, we define the following design criteria to ensure

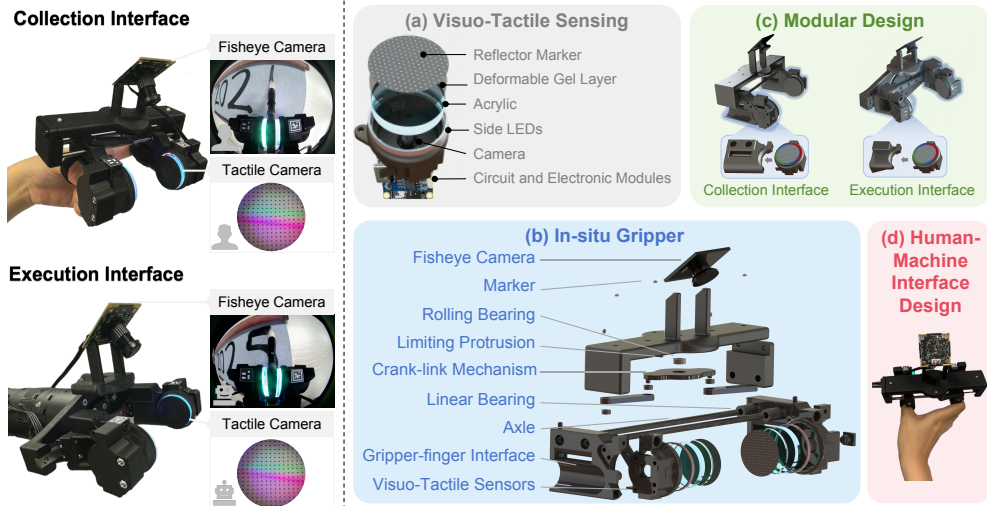


Figure 2: **The hardware system of FreeTacMan.** *Left:* The in-situ gripper in the collection and execution interface respectively, with identical visual and tactile observations. *Right:* (a) Composition of the visuo-tactile sensor. (b) Exploded view of FreeTacMan. (c) The modular design allows for an agile switch between the collection and execution interface. (d) Human-machine interface design.

efficient collection of high-quality visuo-tactile manipulation data with intuitive feedback. **(a)** High-quality visuo-tactile sensing: The designed sensor must achieve competitive sensing performance while minimizing thickness and maximizing the FOV to integration flexibility and enhance spatial perception. **(b)** Efficient data collection: The system should minimize the tactile transmission path from human fingers to the grasped object for real-time and precise tactile feedback, while ensuring stable and fingertip-level dexterous control. **(c)** Scalability: A modular design architecture should be adopted to ensure compatibility across robot embodiments. **(d)** Usability: The system should accommodate a wide range of fingertip sizes, providing ergonomic comfort during operation.

Visuo-Tactile Sensor. As shown in Fig. 2(a), the visuo-tactile sensor integrates the sensing module-comprising circuit and electronic modules, a compact camera, programmable illumination, acrylic, and deformable gel layer-into a single unit, collectively enabling high-fidelity tactile imaging. This module snaps onto the gripper-finger interface via a mechanical connector. Compared to the widely used GelSight Mini [22], our design offers desirable merits in many dimensions, as summarized in Table 2, leading to improved adaptability to diverse robot end-effectors.

In-situ Gripper. FreeTacMan achieves hinge-free operation through visuo-tactile sensors mounted on the operator’s fingertip, where the sensor layer forms the interface between skin and manipulated objects, eliminating intermediate linkages to provide zero mechanical attenuation and natural proprioception. To ensure that the unattenuated tactile feedback directly translates to operator control precision, as illustrated in Fig. 2(b), the system incorporates a linear transmission mechanism with chrome-plated steel shafts and linear bearings, constraining movement to highly accurate linear trajectories (axial deviation ≥ 0.02 mm). Additionally, an inverted crank-slider mechanism converts finger-driven motion into synchronized linear output, while dual parallel shafts and rolling bearings in linking joints minimize friction and lateral torque, achieving over 90% transmission efficiency.

Modular Architecture. FreeTacMan system is built as three plug-and-play modules, each optimized for rapid setup and cross-embodiment compatibility: a sensor perception module for tactile data collection, a universal gripper interface (Fig. 2(c)) for robot compatibility which supports rapid assembly and disassembly of the sensor via a compact mounting mechanism, and a camera mounting scaffold to ensure stable, aligned visual feedback from wrist camera. Customized interfaces are provided for different robot arms, including a 6-DOF Piper arm for low-load tasks and 7-DOF Franka arm for high-precision, heavy-load applications. For 3D models of end-effectors, their integration on different robot arms (e.g., Piper, Franka) and full assembly renders, please visit [our demo page](#).

Table 2: **Comparison between our visuo-tactile sensor and GelSight.** The proposed hardware exhibits several desirable properties, including a higher resolution, FoV, and smaller size in terms of thickness. Though not strictly compared, our design offers a significant cost advantage over the GelSight counterpart (*market price).

Hardware	Resolution Ratio (microns) ↓	FoV (mm ²) ↑	Thickness (mm) ↓	Cost (USD) ↓
GelSight Mini [22]	30 – 100	265.98	28	504*
Ours	15 – 20	358.47	18	30

Human-Machine Interface Design. To achieve rapid adaptability, we incorporate hook-and-loop straps as a fingertip fastening mechanism, as illustrated in Fig. 2(d). These straps accommodate hand sizes ranging from the 5% to 95% percentile of adults and support repeated use [55], balancing operational efficiency. Furthermore, nylon straps offer enhanced breathability and sweat-resistant properties, ensuring user comfort and minimizing the risk of skin irritation during prolonged usage.

3.2 Human-to-Robot Data Transfer

To facilitate human-to-robot skill transfer, a high-precision OptiTrack [56] motion capture system is used for 6D pose tracking of the interface at 300 Hz, achieving a mean error of 0.118 mm. Five retro-reflective markers are mounted on the interfaces, with three positioned on the top plate to measure pose and two on the grippers to capture relative displacement. The coordinates of markers are first transformed from the world coordinate frame to the robot base coordinate frame. A local coordinate frame, aligned with the robot URDF, is established at the gripper’s Tool Center Point (TCP) using three top-plate markers, allowing derivation of end-effector pose while ensuring consistency with the robot kinematic model. We downsample the tracking data to synchronize with RGB images. To this end, each frame contains: the wrist camera RGB image, two visuo-tactile images, the end-effector pose of the in-situ gripper in the world coordinate frame and gripper width. Each trajectory consists of a sequence of such embodiment-agnostic data synchronized at 30 Hz.

Unlike prior works [30, 31] relying on SLAM and IMU fusion to estimate absolute and relative end-effector poses, the motion capture system we have avoids IMU drift and tracking errors. Given the URDF of a target embodiment, we could utilize IKPY [57] as an inverse kinematic solver to map poses of the in-situ gripper to absolute joint positions directly as the action representation.

3.3 Tactile Pretraining and Policy Learning

A two-stage approach is employed to learn visuo-tactile manipulation policies: 1) Tactile representation learning, 2) visuo-tactile policy learning.

Tactile Representation Learning. Our wearable system yields large-scale, contact-rich visuo-tactile trajectories, enabling a high-fidelity dataset for representation learning. Although tactile outputs resemble 2D images, applying a vision encoder pretrained on RGB data often produces suboptimal features due to the domain gap in appearance and semantics [17, 58]. We adopt a CLIP-style [59] contrastive pretraining procedure to bridge the domain gap.

Both the visual encoder f_v and tactile encoder f_t share a ResNet backbone initialized from the same checkpoint. f_v remains frozen during pretraining, while f_t is finetuned. Each encoder is followed by a projection head: g_v for vision, and g_t for tactile, where g_t first concatenates the tactile features with the normalized 7-DOF joint position vector \mathbf{q}_i to inject robot joint state as global context. At each timestep i , we compute the normalized embeddings \mathbf{v}_i and \mathbf{t}_i . We designate \mathbf{v}_i as the *primary positive* for \mathbf{t}_i to align tactile features with the current visual features. However, relying solely on time-aligned contrastive loss neglects temporal dynamics, leading to embeddings that vary abruptly and fail to capture evolving contact patterns. To enforce temporal awareness, a *secondary positive* \mathbf{v}_{i+1} drawn from the next timestep is introduced. All other entries from negatives in a fixed-size

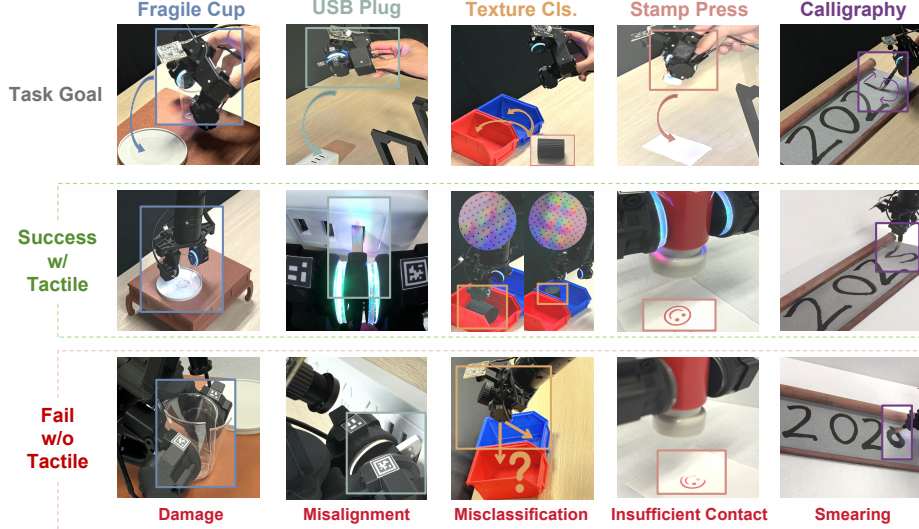


Figure 3: **Human demonstrations and policy rollouts on our tasks.** The top row shows the goal trajectory for each task, while the middle row demonstrates successful rollouts with tactile feedback. The bottom row showcases the typical failure mode of each task when tactile input is absent.

memory bank \mathcal{M} . We train f_t , g_v and g_t by minimizing the following contrastive loss:

$$\mathcal{L} = -\frac{1}{B} \sum_{i=1}^B \log \frac{\exp(\mathbf{v}_i^\top \mathbf{t}_i / \tau) + \exp(\mathbf{v}_{i+1}^\top \mathbf{t}_i / \tau)}{\exp(\mathbf{v}_i^\top \mathbf{t}_i / \tau) + \exp(\mathbf{v}_{i+1}^\top \mathbf{t}_i / \tau) + \sum_{j \in \mathcal{N}_i} \exp(\mathbf{v}_j^\top \mathbf{t}_i / \tau)}, \quad (1)$$

where B indicates batch size, τ is a learned temperature parameter and \mathcal{N}_i indexes the negatives. Please refer to Supplementary Sec. C for pretraining details.

Visuo-Tactile Action Chunking Transformer. We employ the pretrained tactile encoder to extract tactile representations. The vision and tactile embeddings are then concatenated and input into the action chunking transformer (ACT) [11], which is trained to predict absolute joint positions.

4 Experiments

We design experiments to answer three key questions: **Q1.** Can demonstrations be collected efficiently and accurately using FreeTacMan compared to previous setups? **Q2.** Is tactile feedback improving the policy in contact-rich tasks, and how does the policy dynamically integrate visual and tactile information during the execution? **Q3.** What is the benefit of tactile encoder pretraining? How does the temporal-aware CLIP-style contrastive pretraining improve the policy learning?

4.1 Experimental Setup

To answer the questions above, we evaluate the effectiveness of FreeTacMan system and the quality of the collected visuo-tactile demonstration through a diverse set of contact-rich manipulation tasks: 1) **Fragile Cup Manipulation.** The robot grasps a small plastic cup and places it on a tray without causing damage. 2) **USB Plugging.** The robot needs to securely insert a pre-grasped USB plug into a socket. 3) **Texture Classification.** The robot should grasp and identify one of two cylindrical objects with distinct textures and sort it into the correct bin. 4) **Stamp Pressing.** The robot presses a stamp onto paper to produce a clear imprint. 5) **Calligraphy Writing.** The robot traces the digit "5" with a calligraphy brush. 6) **Toothpaste Extrusion.** The robot squeezes a tube to deposit a precise amount of toothpaste. 7) **Tissue Grasping.** The robot lifts a thin tissue from a bag. 8) **Potato Chip Grasping.** The robot picks up a fragile potato chip and places it onto a plate. These tasks cover a wide range of manipulation challenges such as force control, slip detection, and in-hand object pose detection. Five representative tasks are depicted in Fig. 3.

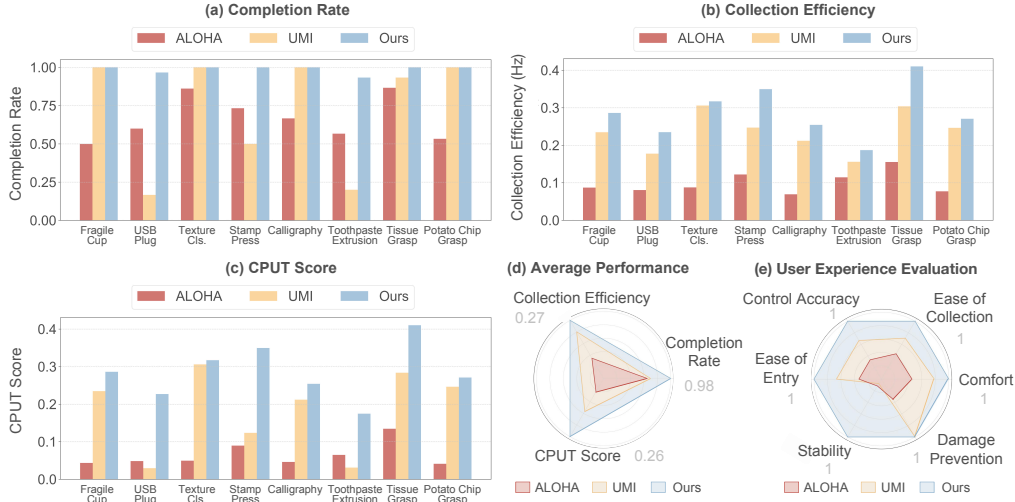


Figure 4: **User Study on data collection.** (a-c) FreeTacMan outperforms ALOHA [27] and UMI [30] in terms of completion rate, collection efficiency, and the CPUT score per task. (d) Average performance of all tasks across three evaluation criteria. (e) FreeTacMan excels at user experience evaluation as well, such as control accuracy, ease of collection procedure, and stability.

4.2 User Study on Data Collection System

Procedure. To answer (Q1), we evaluate the usability of FreeTacMan through a user study including 12 human volunteers, with varying levels of experience in data collection. They collect demonstrations for all 8 tasks. In addition to FreeTacMan, users collect demonstrations using two typical data collection methods: primary–replica-based teleoperation (*i.e.*, ALOHA [27]) and handheld devices (*i.e.*, UMI [30]). To minimize potential biases, no device-specific instructions are provided and each participant conducts three trials with each device for each task. There is no time limit for data collection, but they are instructed to solve tasks as best they can while avoiding collisions and damage. If a task fails, they will continue from where it is interrupted, and the failure will be recorded.

Metrics. We record the task success/failure mode, completion time, and any instances of slippage or damage. Three metrics are adopted to quantify the capability of a particular data collection approach, namely `completion_rate` (fully completed tasks as a percentage of those initiated), `collection_efficiency` (the inverse of data collection time), and an overall score, `Completion per Unit Time` (CPUT), defined as `completion_rate × efficiency`. Additional metrics are reported in the Supp.

Demonstrations could be collected efficiently and accurately using FreeTacMan compared to previous setups (Q1). The results of user study are shown in Fig. 4, where FreeTacMan consistently yields the top completion rate and efficiency. CPUT score in Fig. 4(c) highlights the overall advantage of FreeTacMan, gaining $6.58\times$ higher performance than teleoperation and $7.68\times$ higher than UMI.

For simple tasks which do not require accurate force sensing or control, such as texture classification and tissue grasping, our system and UMI achieve comparable completion rates, while ALOHA performs slightly inferior. In terms of completion time, we have at least a $2.64\times$ advantage over ALOHA and a $1.35\times$ advantage over UMI. In more complex tasks, such as fragile cup manipulation and potato chip grasping, where force feedback is necessary to ensure successful grasping and prevent excessive force, primary-replica teleoperation leads to damage-related failures. This suggests that the handheld method provides better force feedback for grasping delicate objects.

For tasks requiring dynamic force control, such as USB plugging, stamp pressing, and toothpaste extrusion, ALOHA relies on brute force, barely completing them at the risk of causing damage, while UMI often fails due to the lack of slippage detection. In contrast, FreeTacMan combines both precise force perception and control, resulting in superior accuracy and safety. For high-precision trajectory control (*e.g.*, calligraphy writing), ALOHA struggles significantly—users often need to manually

Table 3: **Policy success rates (%) across contact-rich tasks.** The visuo-tactile information, together with the pretraining strategy, greatly helps imitation learning for the contact-rich tasks.

Method	Fragile Cup	USB Plug	Texture Cls.	Stamp Press	Calligraphy	Avg.
ACT [11] (Vision-only)	35	0	20	20	30	21
Ours (+ Tactile w/o Pretraining)	75	10	70	55	65	55
Ours (+ Pretraining)	80	20	90	85	80	71

assist the teaching arm with their other hand, resulting in the longest completion time. While UMI can complete the task, the trajectory smoothness remains inferior to that of FreeTacMan.

Fig. 4(e) summarizes the user experience evaluation. Stability, comfort, ease of collection and entry are assessed via questionnaires and normalized. Stability and damage represent failures of object drops and damage. The results show that FreeTacMan is the most user-friendly and reliable data collection system among the three approaches.

4.3 Validation on Imitation Learning

We collect data and train policies with tasks in Fig. 3 and evaluate each task over 20 trials.

- **ACT [11] (Vision-only):** The baseline ACT uses RGB images from the wrist camera as input only.
- **Ours (+ tactile w/o pretraining):** An extended ACT model taking both visual and tactile observations, which are separately encoded by identical backbones without pretraining.
- **Ours (+ pretraining):** Our full model, where the tactile encoder is pretrained with a multi-positive contrastive objective incorporating both primary and secondary positives.

Integration of tactile feedback results in significant improvement on policy performance, confirming its dynamic value in contact-rich tasks (Q2). The vision-only baseline ACT achieves low performance across all tasks, with an average success rate of 21%. Without tactile feedback, the robot struggles in precise manipulation tasks such as USB plugging and force-sensitive tasks like fragile cup. When tactile feedback is incorporated naively, *i.e.*, without pre-training, performance improves significantly, with the average success rate increasing to 55%. Tasks such as fragile cup handling (75%) and texture classification (70%) gain a remarkable boost over the vision-only baseline. This demonstrates the utility of tactile sensing in tasks that involve contact-rich interactions and visual cues alone are insufficient to distinguish subtle features. However, the performance in tasks like USB plug (10%) and stamp press (55%) still lags behind, indicating room for further refinement.

Temporal-aware pretraining improves the policy performance by aligning visual and tactile embeddings and incorporating temporal dynamics (Q3). Incorporating time-aware visual-tactile pairs in pretraining leads to a notable performance boost, with the average success rate increasing to 71%. As shown in the last line in Table 3, the improvement comes from tasks that demand fine-grained control and the ability to track contact dynamics, such as stamp pressing (85%) and calligraphy (80%). Meaningful gain is witnessed in USB plug (20%). These results show that our approach aligns tactile and visual embeddings while incorporating spatial and temporal context.

5 Conclusion

We present FreeTacMan, a human-centric and robot-free data collection system with in-situ visuo-tactile feedback and recording. A high-quality visuo-tactile sensor is developed, and an in-situ and modular gripper is designed for rapid adaptation. Experimental results demonstrate that the proposed system outperforms existing methods in multiple aspects, including data collection efficiency, control accuracy, and human-machine interaction experience. Through policy validation, the effectiveness of the collected data and the importance of visuo-tactile pretraining are further confirmed.

Limitations

While FreeTacMan has demonstrated efficacy across a range of challenging tasks, a few limitations remain. First, our system currently depends on an external base station for localization. We plan to eliminate this dependency in the future by introducing high-precision visual algorithms, with a continuous focus on reducing hardware reliance and further enhancing system performance. Besides, we have not released a large-scale dataset in this work. However, our data collection system has paved the way to rapidly gather large-scale multi-modal data thanks to its accuracy and efficiency, and we would prioritize this goal in our future work. In addition, we employ a basic policy model, ACT, for downstream validation, but the integration of the visuo-tactile information has not yet been fully investigated. It is worth exploring advanced visuo-tactile sensor fusion algorithms.

Acknowledgments

We gratefully acknowledge Huijie Wang for developing the demonstration page, and Zherui Qiu for assisting with the supervision of the user study. We also thank Yixuan Pan, Qingwen Bu, Zhuoheng Li, Jisong Cai, Yuxiang Lu, and Ningbin Zhang for their valuable insights and constructive discussions. Our appreciation also goes to Zhirui Zhang, Xinyu Yang, Fengjie Shen, Taoyuan Huang, and Lekai Chen for their assistance during the experiments. Finally, we extend our sincere gratitude to all user study participants for their thoughtful feedback.

References

- [1] C. E. Connor and K. O. Johnson. Neural coding of tactile texture: comparison of spatial and temporal mechanisms for roughness perception. *Journal of Neuroscience*, 1992.
- [2] Y. Ikei, K. Wakamatsu, and S. Fukuda. Texture presentation by vibratory tactile display-image based presentation of a tactile texture. In *VRAIS*, 1997.
- [3] T. Yoshioka, S. J. Bensmaia, J. C. Craig, and S. S. Hsiao. Texture perception through direct and indirect touch: An analysis of perceptual space for tactile textures in two modes of exploration. *Somatosens Mot Res.*, 2007.
- [4] W. Xu, Z. Yu, H. Xue, R. Ye, S. Yao, and C. Lu. Visual-tactile sensing for in-hand object reconstruction. In *CVPR*, 2023.
- [5] H. Yousef, M. Boukallel, and K. Althoefer. Tactile sensing for dexterous in-hand manipulation in robotics—a review. *Sensors and Actuators A: physical*, 2011.
- [6] H. Van Hoof, T. Hermans, G. Neumann, and J. Peters. Learning robot in-hand manipulation with tactile features. In *HUMANOIDS*, 2015.
- [7] Z. Su, J. A. Fishel, T. Yamamoto, and G. E. Loeb. Use of tactile feedback to control exploratory movements to characterize object compliance. *Frontiers in Neurorobotics*, 2012.
- [8] W. M. B. Tiest and A. M. Kappers. Cues for haptic perception of compliance. *IEEE Trans. on Haptics*, 2009.
- [9] H.-K. Lee, J. Chung, S.-I. Chang, and E. Yoon. Real-time measurement of the three-axis contact force distribution using a flexible capacitive polymer tactile sensor. *Journal of Micromechanics and Microengineering*, 2011.
- [10] D. Ma, E. Donlon, S. Dong, and A. Rodriguez. Dense tactile force estimation using gelslim and inverse fem. In *ICRA*, 2019.
- [11] T. Z. Zhao, V. Kumar, S. Levine, and C. Finn. Learning fine-grained bimanual manipulation with low-cost hardware. In *RSS*, 2023.
- [12] C. Chi, Z. Xu, S. Feng, E. Cousineau, Y. Du, B. Burchfiel, R. Tedrake, and S. Song. Diffusion policy: Visuomotor policy learning via action diffusion. *IJRR*, 2024.
- [13] S. Liu, L. Wu, B. Li, H. Tan, H. Chen, Z. Wang, K. Xu, H. Su, and J. Zhu. RDT-1B: a diffusion foundation model for bimanual manipulation. In *ICLR*, 2025.

- [14] K. Black, N. Brown, D. Driess, A. Esmail, M. Equi, C. Finn, N. Fusai, L. Groom, K. Hausman, B. Ichter, et al. π_0 : A vision-language-action flow model for general robot control. *arXiv preprint arXiv:2410.24164*, 2024.
- [15] A. Padalkar, A. Pooley, A. Jain, A. Bewley, A. Herzog, A. Irpan, A. Khazatsky, A. Rai, A. Singh, A. Brohan, et al. Open X-Embodiment: Robotic learning datasets and RT-X models. In *ICRA*, 2024.
- [16] Q. Bu, J. Cai, L. Chen, X. Cui, Y. Ding, S. Feng, S. Gao, X. He, X. Huang, S. Jiang, et al. AgiBot World Colosseo: A large-scale manipulation platform for scalable and intelligent embodied systems. *arXiv preprint arXiv:2503.06669*, 2025.
- [17] A. George, S. Gano, P. Katragadda, and A. B. Farimani. Visuo-tactile pretraining for cable plugging. In *ICRA*, 2024.
- [18] T. Lin, Y. Zhang, Q. Li, H. Qi, B. Yi, S. Levine, and J. Malik. Learning visuotactile skills with two multifingered hands. *arXiv preprint arXiv:2404.16823*, 2024.
- [19] B. Huang, Y. Wang, X. Yang, Y. Luo, and Y. Li. 3D-ViTac: Learning fine-grained manipulation with visuo-tactile sensing. In *CoRL*, 2024.
- [20] K. Yu, Y. Han, Q. Wang, V. Saxena, D. Xu, and Y. Zhao. MimicTouch: Leveraging multi-modal human tactile demonstrations for contact-rich manipulation. In *CoRL*, 2024.
- [21] W. Yuan, S. Dong, and E. H. Adelson. GelSight: High-resolution robot tactile sensors for estimating geometry and force. *Sensors*, 17(12), 2017.
- [22] GelSight. Gelsight mini. <https://www.gelsight.com/gelsightmini/>, 2024.
- [23] I. H. Taylor, S. Dong, and A. Rodriguez. GelSlim 3.0: High-resolution measurement of shape, force and slip in a compact tactile-sensing finger. In *ICRA*, 2022.
- [24] S. Chen, C. Wang, K. Nguyen, L. Fei-Fei, and C. K. Liu. ARCap: Collecting high-quality human demonstrations for robot learning with augmented reality feedback. In *ICRA*, 2025.
- [25] C. Wang, H. Shi, W. Wang, R. Zhang, L. Fei-Fei, and C. K. Liu. DexCap: Scalable and portable mocap data collection system for dexterous manipulation. In *RSS*, 2024.
- [26] H. Xue, J. Ren, W. Chen, G. Zhang, Y. Fang, G. Gu, H. Xu, and C. Lu. Reactive Diffusion Policy: Slow-fast visual-tactile policy learning for contact-rich manipulation. In *RSS*, 2025.
- [27] J. Aldaco, T. Armstrong, R. Baruch, J. Bingham, S. Chan, K. Draper, D. Dwibedi, C. Finn, P. Florence, S. Goodrich, et al. ALOHA 2: An enhanced low-cost hardware for bimanual teleoperation. *arXiv preprint arXiv:2405.02292*, 2024.
- [28] Z. Fu, T. Z. Zhao, and C. Finn. Mobile ALOHA: Learning bimanual mobile manipulation with low-cost whole-body teleoperation. In *CoRL*, 2024.
- [29] P. Wu, Y. Shentu, Z. Yi, X. Lin, and P. Abbeel. GELLO: A general, low-cost, and intuitive teleoperation framework for robot manipulators. In *IROS*, 2024.
- [30] C. Chi, Z. Xu, C. Pan, E. Cousineau, B. Burchfiel, S. Feng, R. Tedrake, and S. Song. Universal Manipulation Interface: In-the-wild robot teaching without in-the-wild robots. In *RSS*, 2024.
- [31] Z. Wu, T. Wang, C. Guan, Z. Jia, S. Liang, H. Song, D. Qu, D. Wang, Z. Wang, N. Cao, et al. Fast-UMI: A scalable and hardware-independent universal manipulation interface. *arXiv preprint arXiv:2409.19499*, 2024.
- [32] F. Tao and M. Salmeron. In situ studies of chemistry and structure of materials in reactive environments. *Science*, 2011.
- [33] W. Zheng, P. Chai, J. Zhu, and K. Zhang. High-resolution in situ structures of mammalian respiratory supercomplexes. *Nature*, 2024.
- [34] R. Ding, Y. Qin, J. Zhu, C. Jia, S. Yang, R. Yang, X. Qi, and X. Wang. Bunny-VisionPro: Real-time bimanual dexterous teleoperation for imitation learning. *arXiv preprint arXiv:2407.03162*, 2024.
- [35] T. Buamane, M. Kobayashi, Y. Uranishi, and H. Takemura. Bi-ACT: Bilateral control-based imitation learning via action chunking with transformer. In *AIM*, 2024.

- [36] M. J. Kim, K. Pertsch, S. Karamcheti, T. Xiao, A. Balakrishna, S. Nair, R. Rafailov, E. Foster, G. Lam, P. Sanketi, et al. OpenVLA: An open-source vision-language-action model. In *CoRL*, 2024.
- [37] Y. Zhu, A. Joshi, P. Stone, and Y. Zhu. VIOLA: Imitation learning for vision-based manipulation with object proposal priors. In *CoRL*, 2023.
- [38] K. A. Wyrobek, E. H. Berger, H. M. Van der Loos, and J. K. Salisbury. Towards a personal robotics development platform: Rationale and design of an intrinsically safe personal robot. In *ICRA*, 2008.
- [39] A. Brygo, I. Sarakoglou, N. Garcia-Hernandez, and N. Tsagarakis. Humanoid robot teleoperation with vibrotactile based balancing feedback. In *EuroHaptics*, 2014.
- [40] L. Peternel and J. Babič. Learning of compliant human–robot interaction using full-body haptic interface. *Advanced Robotics*, 2013.
- [41] H. R. Nicholls and M. H. Lee. A survey of robot tactile sensing technology. *IJRR*, 1989.
- [42] Z. Kappassov, J.-A. Corrales, and V. Perdereau. Tactile sensing in dexterous robot hands. *Robotics and Autonomous Systems*, 2015.
- [43] R. S. Dahiya and M. Valle. *Robotic tactile sensing: technologies and system*. Springer, 2013.
- [44] R. S. Dahiya, G. Metta, M. Valle, and G. Sandini. Tactile sensing—from humans to humanoids. *TRO*, 2010.
- [45] Z. He, H. Fang, J. Chen, H.-S. Fang, and C. Lu. FoAR: Force-aware reactive policy for contact-rich robotic manipulation. *RA-L*, 2025.
- [46] Sigma-7. Sigma-7 haptic interface. <https://www.forcedimension.com/products/sigma>, 2024.
- [47] W. Liu, J. Wang, Y. Wang, W. Wang, and C. Lu. ForceMimic: Force-centric imitation learning with force-motion capture system for contact-rich manipulation. In *ICRA*, 2024.
- [48] O. Glauser, D. Panozzo, O. Hilliges, and O. Sorkine-Hornung. Deformation capture via soft and stretchable sensor arrays. *ACM Trans. on Graphics*, 38(2), 2019.
- [49] T. Hellebrekers, O. Kroemer, and C. Majidi. Soft magnetic skin for continuous deformation sensing. *Advanced Intelligent Systems*, 2019.
- [50] R. Bhirangi, T. Hellebrekers, C. Majidi, and A. Gupta. ReSkin: versatile, replaceable, lasting tactile skins. In *CoRL*, 2021.
- [51] R. Bhirangi, V. Pattabiraman, E. Erciyes, Y. Cao, T. Hellebrekers, and L. Pinto. AnySkin: Plug-and-play skin sensing for robotic touch. In *CoRL*, 2024.
- [52] Y. Yan, Z. Hu, Z. Yang, W. Yuan, C. Song, J. Pan, and Y. Shen. Soft magnetic skin for super-resolution tactile sensing with force self-decoupling. *Science Robotics*, 6(51), 2021.
- [53] E. Donlon, S. Dong, M. Liu, J. Li, E. Adelson, and A. Rodriguez. GelSlim: A high-resolution, compact, robust, and calibrated tactile-sensing finger. In *IROS*, 2018.
- [54] J. Ren, J. Zou, and G. Gu. MC-Tac: Modular camera-based tactile sensor for robot gripper. In *ICIRA*, 2023.
- [55] A. C. Zoeller and K. Drewing. A systematic comparison of perceptual performance in softness discrimination with different fingers. *Attention, Perception, & Psychophysics*, 2020.
- [56] OptiTrack. Optitrack. <https://optitrack.com/>, 2024.
- [57] P. Manceron. IKPy. <https://github.com/Phylliade/ikpy>, 2016.
- [58] F. Liu, C. Li, Y. Qin, A. Shaw, J. Xu, P. Abbeel, and R. Chen. ViTaMin: Learning contact-rich tasks through robot-free visuo-tactile manipulation interface. *arXiv preprint arXiv:2504.06156*, 2025.
- [59] A. Radford, J. W. Kim, C. Hallacy, A. Ramesh, G. Goh, S. Agarwal, G. Sastry, A. Askell, P. Mishkin, J. Clark, et al. Learning transferable visual models from natural language supervision. In *ICML*, 2021.

Supplementary Material

A Hardware Design

| Supplement to Sec. 3.1 in the Main paper.

Hardware Implementation Details. The sensor is rigidly connected to the gripper base via a primary threaded hole, bearing the main mechanical load. On the opposite side, a protruding feature fits precisely into a corresponding groove on the gripper base, enabling straightforward plug-in alignment and positioning. Additional constraint is provided by auxiliary screws on the rear side to prevent damage from vibration or impact, further enhancing stability.

For visual perception, we use a fisheye camera equipped with a 180° field-of-view lens, capturing video at 30 frames per second with a resolution of 640×480 pixels. The tactile sensor is integrated with a camera operating at 30 FPS with a resolution of 640×480 pixels. Designed with custom 3D-printed parts and commercially available standard components, the system achieves a lightweight ($157.5g$) and compact ($145 \times 85 \times 106mm^3$) form factor, ensuring portability and reproducibility.

Seamless Integration into Robotic Platforms. Fig. 5 illustrates the universal gripper interface with quick-swap mounts compatible with both the Piper and Franka arms, as well as the camera scaffold designed for precise alignment with the wrist-mounted camera to ensure consistent perspective. These components demonstrate the plug-and-play modularity of FreeTacMan, enabling seamless integration across diverse robotic platforms without requiring hardware-specific modifications.

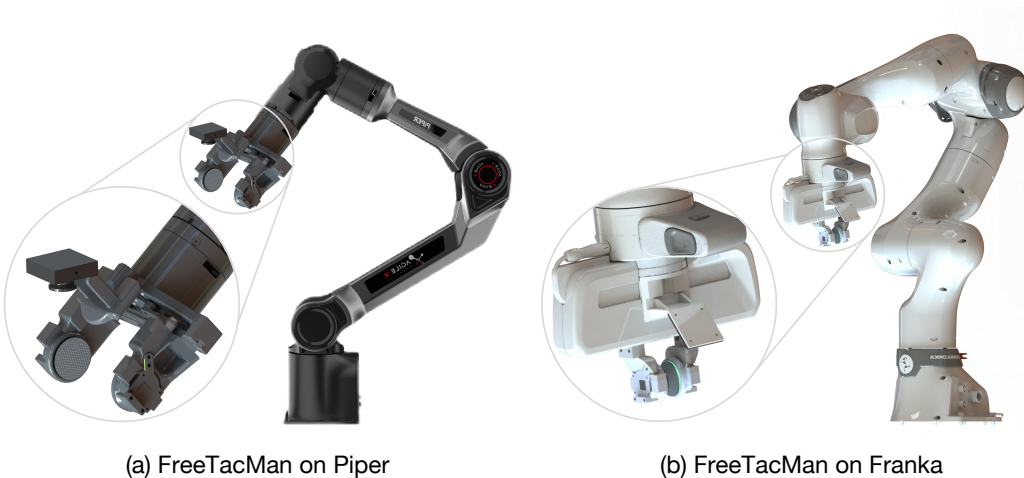


Figure 5: **Detailed mounting interface for different robot arms.** (a) and (b) illustrate the integration of FreeTacMan with the PIPER and Franka robotic arms, respectively. The zoomed-in views highlight the connector regions and camera mounting positions, which are carefully aligned to maintain a consistent viewpoint between the data collection and execution systems.

B Data Processing

| Supplement to Sec. 3.2 in the Main paper.

Fig. 6 elaborates on coordinate transformation for demonstration-to-execution consistency. During human demonstration, the OptiTrack system defines a global coordinate frame, which differs from the robot’s base frame used during inference. To ensure consistency, the positions of the five markers are transformed—via rotation and translation—into the robot’s base frame for accurate task execution. To obtain the robot end-effector pose—necessary for subsequent joint angle computation—a local coordinate frame is established with the Tool Center Point (TCP) as its origin. All coordinate frames

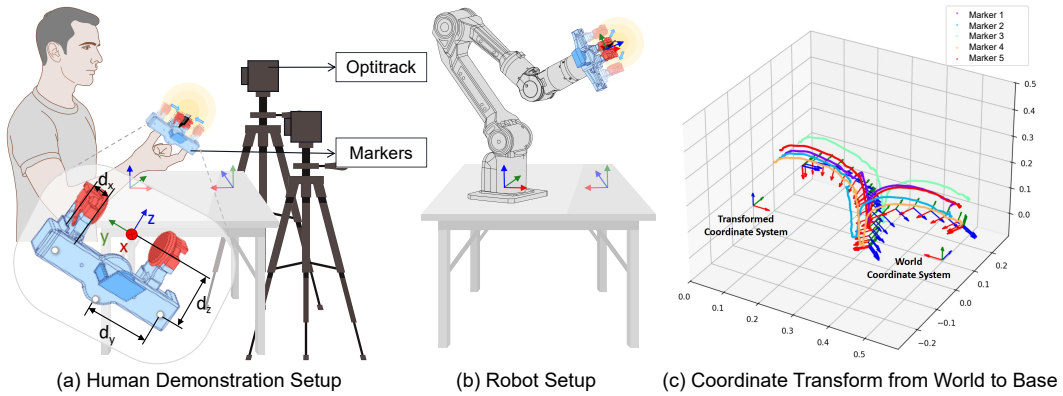


Figure 6: **System setup and coordinate transformation for human demonstration and robot execution.** (a) Human demonstration setup showing the OptiTrack-defined world frame, the robot base frame, and the local frame on the data collection device. (b) Robot setup with the base at the origin and a local frame consistent with the demonstration. (c) Coordinate transformation example for texture classification task, visualizing five marker trajectories and the local frame in 3D space.

follow the right-hand Cartesian convention. The position of TCP is determined using three markers mounted on the top plate. Among these, the two with the greatest distance define the direction of the dy axis, while the dx axis points from the third marker to the midpoint of the other two. The magnitude of dy is set to half the distance between the two farthest markers. The dx and dz offsets, defined by hardware dimensions, represent the TCP’s position relative to the two front-facing markers. During task execution, this local coordinate frame remains aligned with the one defined during data collection. Fig. 6(c) illustrates an example of coordinate transformation in a texture classification task, visualizing the trajectories of five markers and the local frame in 3D space.

C Training Details

| *Supplement to Sec. 3.3 in the Main paper.*

Problem Formulation. We define a visuo-tactile manipulation policy for the robot as a mapping $\pi : \mathcal{O} \rightarrow \mathcal{A}$, where the observation space \mathcal{O} consists of three modalities: visual observation $\mathbf{o}_t^v \in \mathcal{O}^v \subset \mathbb{R}^{H \times W \times 3}$, tactile observation $\mathbf{o}_t^t \in \mathcal{O}^t \subset \mathbb{R}^{H \times W \times 3}$, and robot proprioception $\mathbf{o}_t^r \in \mathcal{O}^r \subset \mathbb{R}^{n_s}$ as $\mathbf{o} = (\mathbf{o}_t^v, \mathbf{o}_t^t, \mathbf{o}_t^r)$. The action space $\mathbf{a} \in \mathcal{A} \subset \mathbb{R}^7$ is defined as 6-DoF arm joint position and 1-DoF gripper position. The policy π is learned via imitation learning to map these observations to corresponding actions.

Details on Tactile Pretraining. We pretrain the tactile encoder f_t and projection head g_v, g_t using a CLIP-style contrastive loss with multi-positive sampling. Optimization is performed using AdamW with cosine-annealed learning rates, updating only the tactile encoder f_t , visual g_v , and tactile projection g_t while keeping visual encoder f_v fixed. We train on the sequence of time-aligned visuo-tactile frames, drawing primary positives from the same timestep and secondary positives from

Table 4: Hyperparameters for tactile pretraining.

Hyperparameters	Value
Visual backbone	ResNet-18 (Frozen)
Tactile backbone	ResNet-18 (finetuned)
Projection dimension	256
Learning rate	$1e - 4$
Batch size	128

Table 5: Hyperparameters for policy learning.

Hyperparameters	Value
Visual RGB resolution	640×480
Tactile RGB resolution	640×480
Chunk size	48
Hidden dimension	512
Visual backbone	ResNet-18
Tactile backbone	ResNet-18 (Pretrained)
Learning rate	$4e - 5$
Weight decay	$1e - 4$
Batch size	64
KL weight	10

the next frame (with wrap-around). Negatives are sampled from a memory bank of size 4096. Table 4 shows the hyperparameters of pretraining.

Details on Policy Learning. We adopt the action chunking transformer (ACT) [11] architecture to learn visuo-tactile manipulation policies. Both visual and tactile images are 640×480 pixels and fed as stacked inputs to the ACT backbones. At each timestep, the model outputs an action chunk of length \mathcal{T} , where each action in the chunk specifies a 6-DOF joint action for robot arm plus a 1-DOF gripper action. To integrate our visuo-tactile pipeline, we add our pretrained tactile encoder f_t to extract tactile features. The tactile features are concatenated with visual features and input into the transformer encoder of ACT. Table 5 shows the hyperparameters of policy learning.

D Experimental Setup

| *Supplement to Sec. 4.1 in the Main paper.*

Task Specification. We present a comprehensive description of each task below.

- **Fragile Cup Manipulation.** In this task, the robot is required to grasp a small plastic cup from a rack and place it into a tray on the rack. A trial is considered successful if the cup is stably placed within the tray without any damage or visible deformation to the cup. This task is designed to evaluate the role of tactile feedback in delicate object handling.

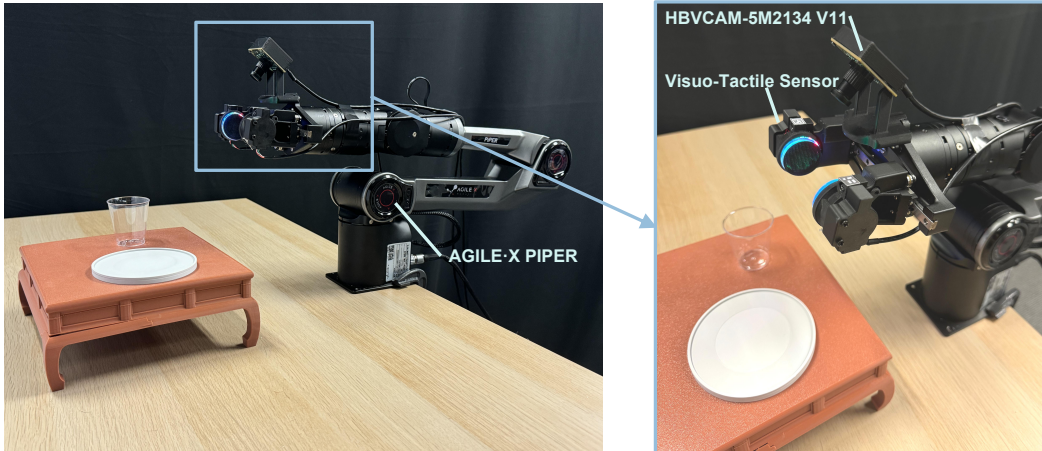


Figure 7: **Experiment setup for policy deployment.** The sensing system, consisting of a fisheye camera and two tactile sensors, is mounted on the end effector in the same configuration used during data collection.

- **USB Plugging.** The robot must insert a pre-grasped USB into a specified socket on a power strip for this task. A success is recorded if the USB is inserted to a sufficient depth such that it remains securely connected. Tactile information serves as an additional signal to assist with fine alignment.
- **Texture Classification.** This task involves recognizing and sorting two types of cylindrical objects, each covered with distinct industrial-grade surface textures. The robot must grasp an object, identify its texture through visuo-tactile perception, and place it into the correct bin corresponding to the texture type. Tactile sensing provides direct information for surface material recognition.
- **Stamp Pressing.** In the stamping task, the robot needs to press a pre-grasped circular stamp onto a sheet of paper laid flat on the table. The task is deemed successful if a clear and complete imprint of the stamp is produced on the paper surface. The stamping task leverages tactile feedback to control contact force during imprinting.
- **Calligraphy Writing.** For the calligraphy brush writing task, the robot must use a pre-grasped calligraphy brush to trace the digit "5" following a guide labeled "202" on a piece of cloth. A success is determined if the resulting written pattern can be visually recognized and interpreted as the number "5". In this task, tactile information helps the robot estimate the in-hand brush pose during fine motion.
- **Toothpaste Extrusion.** This task requires the robot to extrude toothpaste from a pre-grasped tube onto a sheet of paper placed on the table. The task is considered successful if the toothpaste is deposited on the paper in an amount consistent with typical daily use for brushing. Tactile feedback helps the robot modulate the applied force, ensuring the right amount of toothpaste is dispensed.
- **Tissue Grasping.** The robot is tasked with extracting a single tissue from a box. A trial is considered successful if the tissue is pulled out without slipping. Tactile sensing provides real-time feedback to confirm initial contact and ensure a stable grasp throughout the pulling motion.
- **Potato Chip Grasping.** In this task, a fragile potato chip—slightly larger in diameter than a plastic cup—is placed atop the cup. The robot must grasp the chip and transfer it to a nearby dish without touching the cup or breaking the chip. A trial is deemed successful if the chip is placed intact into the dish. Tactile sensing plays a critical role in confirming secure contact with the chip while avoiding excessive force that could lead to breakage.

Implementation Details. We conduct all experiments on a PIPER 6-DOF light-weight robotic arm (AGILE-X Robotics) equipped with our FreeTacMan mounted at the wrist, as shown in Fig. 7. The robot is connected to a workstation running Ubuntu 20.04 and ROS Noetic on an NVIDIA RTX 4090 GPU. RGB frames are captured at 30 Hz by HBVCAM fisheye camera and published via ROS topics, and tactile frames from our camera-based tactile sensor are sampled at 30 Hz. Our imitation policy performs inference on the GPU, with policy latency averaging under 20 ms per cycle.

Evaluation Metrics in User Study. We provide detailed explanations of the evaluation metrics used for User Experience Evaluation.

- **Comfort and Ease of Collection:** After completing all eight tasks with each of the three systems, participants rated how physically comfortable it was to perform the demonstrations on a scale from 1 (very uncomfortable) to 5 (very comfortable). In the same survey, they scored the ease of collection from 1 (very difficult) to 5 (very easy).
- **Ease of Entry:** After using all three systems, participants ranked them in order of entry difficulty. We convert these rankings into a normalized score where a lower average rank corresponds to a higher ease-of-entry value.
- **Control Accuracy:** Volunteers ordered the three systems by how precisely they could control the gripper during demonstrations. These ranks are normalized so that a lower mean rank indicates higher control fidelity.
- **Stability and Damage Prevention:** During each demonstration, we logged the number of times the prop slipped from the gripper and the number of times the prop was visibly deformed or damaged.

All metric values are normalized, with higher scores indicating better performance, as visualized by the radar chart shown in Fig. 4(e) in the main paper.

Table 6: **Detailed results of user study.** FreeTacMan outperforms existing data collection methods across seven manipulation tasks. **Completion Rate** is the fraction of successful demonstrations; **Time** is the average collection duration; **Slip Count** and **Damage Count** record object slips and damages during collection; **Performance** is an overall metric combining efficiency and reliability.

Task	Method	Comple. Rate	Task Duration (s)	Slip Count	Damage Count	CPUT Score
Texture Class.	ALOHA	0.8611	11.41	5	0	0.0495
	UMI	1.0000	3.27	0	0	0.3060
	Ours	1.0000	3.15	0	0	0.3171
Fragile cup	ALOHA	0.4997	11.48	2	14	0.0435
	UMI	1.0000	4.26	0	0	0.2348
	Ours	1.0000	3.49	0	0	0.2863
USB Plug	ALOHA	0.5997	12.40	9	0	0.0484
	UMI	0.1665	5.63	27	0	0.0296
	Ours	0.9666	4.26	2	0	0.2270
Calligraphy Writing	ALOHA	0.6664	14.44	2	0	0.0461
	UMI	1.0000	4.72	2	0	0.2120
	Ours	1.0000	3.93	0	0	0.2543
Stamp Pressing	ALOHA	0.7330	8.18	3	2	0.0896
	UMI	0.4997	4.05	26	0	0.1235
	Ours	1.0000	2.86	1	0	0.3497
Toothpaste Dispensing	ALOHA	0.5665	8.73	16	0	0.0649
	UMI	0.1998	6.41	6	0	0.0312
	Ours	0.9332	5.34	1	0	0.1746
Tissue Grasping	ALOHA	0.8665	6.44	5	0	0.1346
	UMI	0.9332	3.29	3	0	0.2837
	Ours	1.0000	2.44	0	0	0.4103
Chip Grasping	ALOHA	0.5330	12.94	5	4	0.0412
	UMI	1.0000	4.06	0	0	0.2464
	Ours	0.9666	3.69	1	0	0.2617

E Additional Experiments

Evaluation on User Study. Table 6 reports completion rate, task duration, slip count, damage count and CPUT for each method across our eight contact-rich tasks.

- **Completion Rate:** Across all tasks, FreeTacMan achieves the highest completion rates, reaching 100% (Texture class, Fragile cup, Stamp pressing, Tissue grasping, Calligraphy) or near-perfect rates (USB plugging, Chip grasping, Toothpaste dispensing). In contrast, ALOHA’s rates range from 49.97% (Fragile cup) to 86.65% (Tissue grasping), and UMI’s range from 16.65% (USB plug) to 100% (Calligraphy, Chip grasping). This demonstrates that real-time tactile feedback enhances the human operator’s ability to execute and complete precise, contact-rich tasks.
- **Task Duration:** FreeTacMan demonstrates the shortest task durations, averaging between 2.44s (Tissue grasping) and 5.34s (Toothpaste dispensing). UMI’s times range from 3.29s to 6.41s, while ALOHA’s are substantially higher (6.44s to 14.44s). Handheld paradigm outperforms ALOHA in data collection efficiency due to its intuitive feedback, while in-situ feedback of FreeTacMan leads to faster data collection.
- **Slip and Damage Count:** High slip counts indicate poor force and slippage feedback. ALOHA records up to 27 slips (USB insertion) and 14 damages (Fragile cup), reflecting its indirect force perception. UMI improves the force feedback and records zero damage events, yet its multi-link transmission still permits noticeable slippage in force-sensitive tasks (e.g., 26 slips during Stamp pressing). In contrast, FreeTacMan limits slips to at most 2 and records zero damage across all tasks, evidencing its high-fidelity, low-latency tactile feedback.

- **CPUT:** As a combined metric of efficiency and reliability, CPUT highlights the overall advantage of FreeTacMan: it achieves scores from 0.1746 (Toothpaste dispensing) to 0.4103 (Tissue grasping), substantially outperforming ALOHA and UMI. For tasks like Stamp pressing, the CPUT of FreeTacMan reaches 0.3497, which exceeds ALOHA and UMI by nearly 3 times, confirming its advantage under precise contact requirements.

Overall, these results indicate that in-situ design of FreeTacMan improves both the accuracy and efficiency of human-operated data collection in contact-rich tasks.

Evaluation of Visuo-tactile Modality Fusion. To understand how our policy integrates visual and tactile inputs, we extract and visualize both the decoder’s cross-attention and the encoder’s self-attention maps during inference. After running the model forward, we compute the cross-attention and self-attention via registered forward hooks. Specifically, the cross-attention from the ACT decoder is

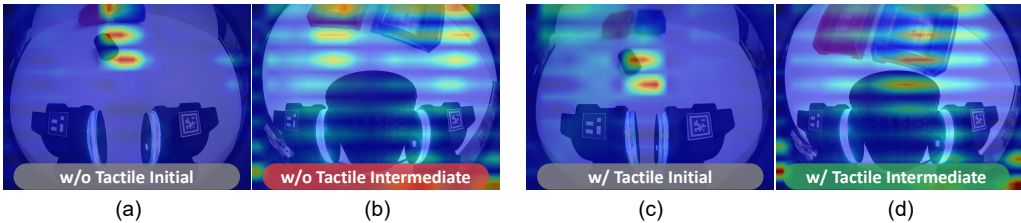


Figure 8: **Visual Attention Heatmaps in Texture Classification.** Cross-attention overlays on the visual input: Left two panels (Vision-only ACT): (a) before grasp and (b) after grasp. Right two panels (Visuo-tactile ACT): (c) before grasp and (d) after grasp.

captured by averaging across heads, resulting in a single importance vector of length S . This vector is then divided into visual and tactile portions, with each reshaped to its spatial layout and upsampled to the original image resolution for overlay. The encoder self-attention is captured from the attention heads, then the averaged self-attention is reshaped and overlaid onto visual and tactile images.

Fig. 8 shows the decoder cross-attention overlays on the visual input during the texture classification task. In the first row, we show two snapshots from the vision-only ACT model: the left image is at the initial state of inference, where attention is correctly focused on the target cylindrical object; the right image is after the gripper has lifted the object, the model’s attention is diffusely allocated to both the red and blue bins due to the lack of tactile cues. In the second row, we show the corresponding stages for our model with tactile integration: initial attention in the left image is on the target object again, but after lift (right), the model uses tactile feedback to recognize texture and concentrates its attention exclusively on the correct (blue) bin. This comparison demonstrates how tactile information refines the decision of policy during inference.

Fig. 9 depicts how the ACT model’s decoder cross-attention shifts over the tactile image during inference of texture classification. The left image shows the attention map just before the gripper

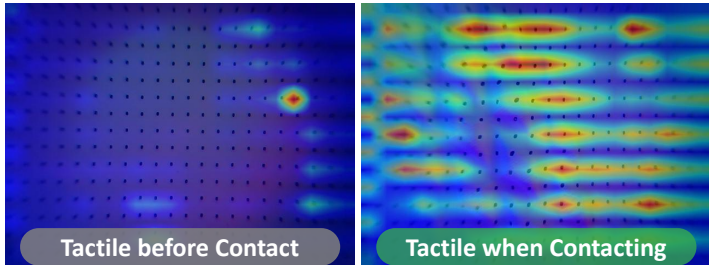


Figure 9: **Attention heatmap on tactile images.** We overlay the decoder’s cross-attention on tactile images during inference of texture classification. **Left:** at the initial state, the attention is spread across the gel surface, **Right:** after contact, the attention focuses on the region of deformation.

makes contact: since no deformation has happened, attention is broadly distributed over the gel layer. In contrast, the right image captures the moment immediately after contact, where the model concentrates its attention on the region of deformation that corresponds to the object's surface texture. This dynamic reallocation of attention enables the policy to detect fine-grained tactile cues and infer both texture and object geometry in real time.